

Study of strong cross-field sheared flow with the vorticity probe in the Large Plasma Device

Jean C. Perez^{a,*} W. Horton^{a,†} Roger Bengtson^{b,‡} and Troy Carter^{c‡}

^a*Institute for Fusion Studies*

^b*Fusion Research Center*

University of Texas at Austin

Austin, Texas, 78712, USA

^c*University of California, Los Angeles*

Los Angeles, California, USA

(Dated: November 4, 2005)

Abstract

We report evidence for the existence of coherent structures created by the Kelvin-Helmholtz instability in steady-state, shear-flow driven plasmas in the Large Plasma Device (LAPD) facility at UCLA. The measurements are performed with the Vorticity Probe (VP), a newly designed probe that directly measure the plasma vorticity associated with the $\mathbf{E} \times \mathbf{B}$ shear flow by means of a method that is both simpler and more accurate than the methods used in neutral fluids. Because the rate of change of vorticity is a key quantity in nonlinear models, like in Hasegawa-Mima equation, its direct measurement is critical for verification purposes. The physical origin of the rate of change of plasma vorticity from $\mathbf{E} \times \mathbf{B}$ flow is the divergence of the ion polarization current. Vortex coherent structures occur when the vorticity is a nonlinear function of the stream function (which for magnetized plasmas is the electric potential divided by the magnetic field strength). A strong-shear-flow regime in the LAPD was used to create the Kelvin-Helmholtz instability.

The work was supported under the U.S. Department of Energy contract DE-FG02-04ER 54742.

*Electronic address: jcperez@physics.utexas.edu

†Electronic address: horton@physics.utexas.edu

‡Electronic address: bengtson@physics.utexas.edu

I. INTRODUCTION

It is widely known that vorticity plays a significant role in the nonlinear dynamics of neutral fluids and plasmas. For instance, Navier-Stokes equation has alternative formulations in terms of the fluid vorticity [1–3], which is defined as

$$\boldsymbol{\omega} \equiv \nabla \times \mathbf{v} \quad (1)$$

Same definition follows in fluid-like plasma equations, like MHD, and generalized magnetofluid models, from which reduced sets of equations can be obtained for specific plasma conditions. The most well know of these models are the one field Hasegawa-Mima equation [4], the two fields Hasegawa-Wakatani [5] equations, Hamaguchi-Horton model [6], ETG, ITG, etc. The common feature of these models, the rate of change of vorticity, has its origin in the divergence of the plasma polarization current that provides the charge balance in the quasineutral plasma. Therefore, it is essential to measure vorticity for the validation and quantitative understanding of these models, in which one of the equations is

$$\frac{d}{dt}\omega = \left(\frac{\partial}{\partial t} + \mathbf{v}_E \cdot \nabla \right) \omega = S_\omega(x, t) \quad (2)$$

The physical origin of sources and sinks S_ω depends on the specific model and can act as a coupling term to other relevant dynamical fields. Due to the incompressibility of the $\mathbf{E} \times \mathbf{B}$ flow, Eq. (2) is a statement of local vorticity conservation.

Nowadays, to the best of our knowledge, measurements of vorticity are indirectly obtained from fluid velocimetry, that is, vorticity is calculated by a process of finite differences on measured flow fields. One of the main disadvantages of this process is that it is prone to inherent errors in the numerical schemes used in obtaining the curl of the velocity field. In this work, we make use of the vorticity probe design, introduced in [7]. This vorticity probe takes advantage of the fact that in a strongly magnetized plasma, the streamfunction associated to the dominant $\mathbf{E} \times \mathbf{B}$ flow is proportional to the plasma electrostatic potential as expressed in the equation

$$\mathbf{v}_E = \frac{\mathbf{E} \times \mathbf{B}}{B^2} = \frac{\mathbf{e}_z \times \nabla \varphi}{B} \quad (3)$$

where we have taken $\mathbf{B} = B\mathbf{e}_z$. In terms of the stream function, the magnetic-field-aligned vorticity is

$$\omega_z = \frac{1}{B} \nabla_{\perp}^2 \varphi. \quad (4)$$

From this equation we can see that plasmas in which the $\mathbf{E} \times \mathbf{B}$ is the dominant flow have two advantages over neutral fluids: (1) the stream function field can be obtained by measuring plasma potential, (2) the finite difference scheme is to be applied to a scalar rather than to a vector field, then measuring vorticity under these conditions is both simpler and more accurate, provided equation Eq. (4) holds.

The vorticity probe design and use is discussed in [7] in the context of Kelvin-Helmholtz turbulence generated in the Large Plasma Device (LAPD) facility at UCLA.

This paper is organized as follows. Section II is devoted to a general description of the experiment, section IIA describes the sheared flow regimes obtained under the experimental conditions, in section IIB we report measurements of vorticity fluctuations and probability distribution functions obtained from the data. Section IIC shows standard spectral two point correlation analysis to find evidence of propagating modes. Finally section III shows comparison of the measured wave characteristic with the available linear theories available in the literature. Section IV we conclude.

II. EXPERIMENT ON LARGE PLASMA DEVICE

We present measurements from the vorticity probe in the upgraded Large Plasma Device [8] at the University of California, Los Angeles (UCLA). LAPD is 18 m in length, with a plasma column ~ 0.8 m in diameter created by a pulsed discharge ~ 20 ms long from a Barium Oxide coated emissive cathode. The plasma parameters for these experiments were $n_e \sim 1.2 \times 10^{18} \text{ m}^{-3}$, $T_e \sim 10$ eV and $B \sim 0.08$ T with helium as the working gas. Background neutral density at the position of the probe measurements is less than 10^{12} m^{-3} as determined by spectroscopic measurements and which is consistent with measured pressures in LAPD. This level of neutral background gives a small ion-neutral collision frequency of order 100 /s. These collisions provide a small background viscosity that is negligible for the wavenumbers considered here.

A. Sheared flow regimes

A sheared poloidal velocity profile is established by biasing the chamber wall with respect to the anode and cathode (see Fig. 1) for 5 ms during the discharge. This biasing results

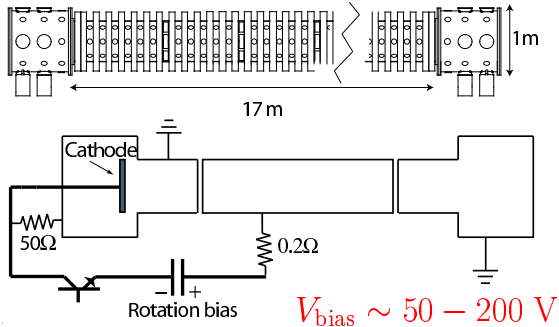


FIG. 1: Schematic of the Large Plasma Device (LAPD), including a diagram of the circuit used for plasma column biasing.

in different sheared $\mathbf{E} \times \mathbf{B}$ flow turbulent regimes at the edge of the plasma column. We can classify these regimes according to the dominant instability that drives the turbulence as shown in table I.

	Kelvin-Helmholtz	Drift-Wave+KH	Drift-Wave
E_r	~ 1.5 kV/m	~ 0.4 kV/m	Weak
v_E	~ 10 km/s	~ 5 km/s	Slow
ρ_s	~ 10 mm	~ 5 mm	same
v_{de}	~ 0.6 km/s	~ 1.5 km/s	same

TABLE I: Sheared flow regimes arising from wall biasing experiments. These regimes are classified according to the instability that is believed to drive the turbulence

Fig. 2a shows the background mean profiles for the first of these regimes, the MHD Kelvin-Helmholtz in which the $\mathbf{E} \times \mathbf{B}$ dominates the perpendicular dynamics with weak coupling to the parallel direction. In this case potential fluctuation levels are significantly higher than density fluctuations, $e\phi/T_e \gg \delta n/n$. The mode spectrum and vorticity statistic is reported in [7]. The third regime for which there was no available data at this time is one of very weak shear with steep density gradient driven drift wave turbulence. Fig. 2b shows the second regime, a hybrid Drift-Wave Kelvin-Helmholtz in which both mechanisms are believed to drive the turbulence. This regime, with a significant drift wave component shows the clearest formation of the internal transport barrier in the density profile as would be expected.

Fig. 3a shows the background $\mathbf{E} \times \mathbf{B}$ flow as calculated from the plasma potential estimated from the floating potential and temperature measurements from the triple probe for the strong shear conditions [Kelvin-Helmholtz]. Fig 3b shows the $\mathbf{E} \times \mathbf{B}$ flow from the triple probe measurements compared Mach probe measurements. The agreement between the triple probe estimates of flow velocity and Mach probe measurements is not as good as might be desired, but both velocities show the same profile, with some differences in velocity scale. If the mach probe plot were to be recalibrated by using the $\mathbf{E} \times \mathbf{B}$ data, both curves will have good agreement, except in the region where the density gradient is significant, with the difference being of the order of the diamagnetic drift velocity associated to this density gradient. These measurements put our assumptions on the perpendicular flows on firm grounds, and consequently the accuracy of the measurement of vorticity fluctuations with the vorticity probe.

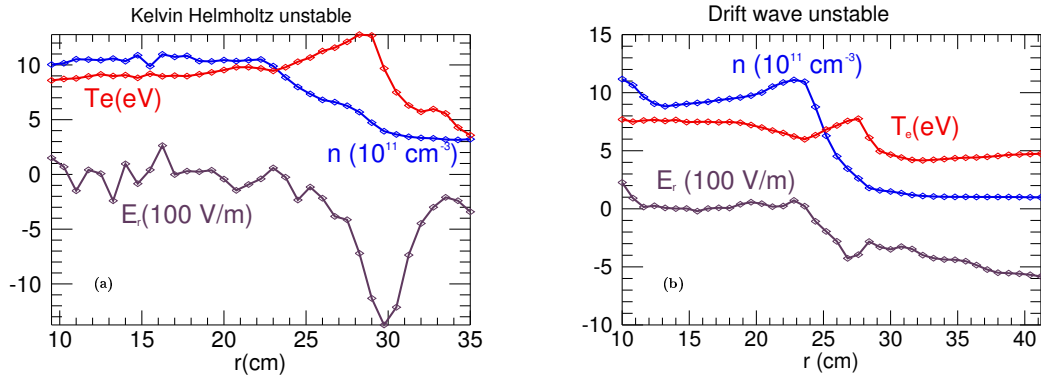


FIG. 2: Mean profiles obtained as an average in 25 experimental shots during the stationary turbulent state during the wall-bias pulse.

B. Vorticity fluctuations

Vorticity fluctuations are obtained from the vorticity probe shown in Fig. 4. The principle behind the vorticity probe is the use of Langmuir probes in the stencil of discrete approximation of the Laplacian used in numerical computations, see for instance [9]. The vorticity probe tips are oriented along the direction of the magnetic field (into the page in Fig. 4). The central five tips are arranged in a diamond pattern, with the outer four tips separated from the central tip by 5 mm. The five inner tips are used to measure the floating potential,

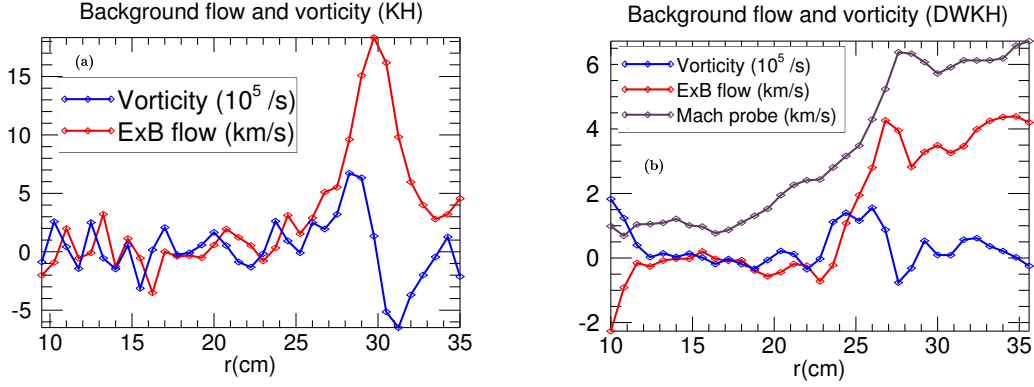


FIG. 3: $\mathbf{E} \times \mathbf{B}$ flow constructed from the average electric field during the wall bias pulse and the vorticity associated with it. Top: Kelvin-Helmholtz regime, Bottom: Drift Wave+KH regime.

which is then used to compute a finite difference value of the vorticity. For this, four times the floating potential on the central tip must be subtracted from the floating potential on the surrounding four tips. During biased rotation experiments in LAPD, the DC floating potential can reach values of order 200V, substantially larger than the observed fluctuation amplitude (~ 1 V). The floating potential measurements are therefore performed using AC coupled amplifiers in order to reject the large low-frequency floating potential signal and to maximize the use of the dynamic range of the available digitizers.

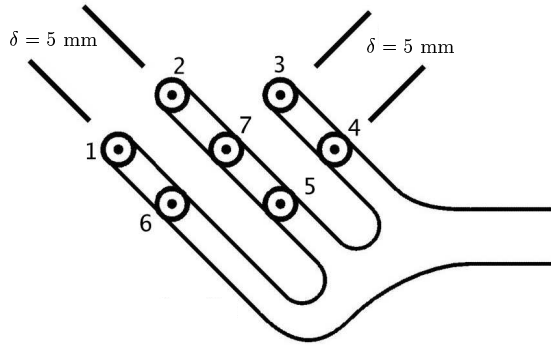


FIG. 4: Vorticity probe design. The probe is inserted into the LAPD plasma radially, so that the magnetic field is perpendicular to the surface of the probe tips and points out of the page.

The vorticity probe is scanned along the radius at 51 positions. At each location 25 experimental shots are taken with a sampling rate of 100 MSamples/s, leading to 28672 time points per radius and shot.

Fig. 5 shows probability distributions functions (PDFs) associated with vorticity at every measured radial location as compared to a Gaussian distribution represented by the solid line. The vorticity pdfs are obtained from 102400 vorticity samples as a result of combining 25 experimental shots with 4096 time points each during the bias pulse. Vorticity PDFs show the intermittent character of vorticity through heavy tails in both regimes, which we associate to the existence of coherent structures present in the shear layer. The main qualitative difference between both regime is the skewness of the PDFs. In the KH regime the skewness of the PDFs as one moves across the shear region presents evidence of a chain of counter rotating vortices consistent with the sign of the background vorticity. The DWKH regime does not show this antisymmetry, as we expect from the symmetric form of the background vorticity.

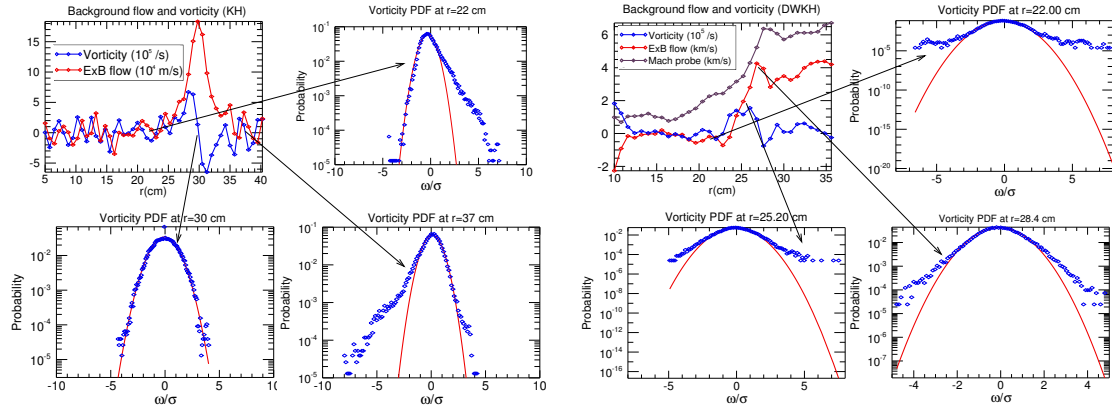


FIG. 5: Vorticity probability distribution functions for representative radius in each reported regime. PDF are constructed with vorticity fluctuation measurements from 25 experimental shots at each radius during the bias pulse, for a total of 102400 samples.

The skewness of the vorticity PDF in Fig. 5 with positive, counterclockwise rotating plasma vortices inside the maximum of the jet, $v_{max} \sim 20$ km/s at $r = 30$ cm shown in Fig. 2a and clockwise rotating vortices outside the maximum of $v_{\theta}(r)$ is the standard result of patches of alternating sign vortices from a localized jet.

This configuration follows from the conservation of angular momentum and mass. Simulations show that like regions of vorticity with the same direction of rotation are strongly merging. Thus we may expect larger scale vortices to form in the nonlinear fluctuation spectrum.

C. Two points spectral analysis

Using standard one and two point correlation techniques [10, 11] with selected tips of the vorticity probe, wave characteristics can be obtained at different radial positions. Fig. 6a shows the auto power spectrum for the plasma potential from the central tip 7 (see Fig. 4) at probe position $r = 28.4$ cm, corresponding to the center of the shear layer. The turbulent spectrum during the bias pulse is dominated by frequencies in the range from 5 to 50 kHz. Cross phase between two angularly separated probes, shown in figure 6b, can be used to identify the azimuthal mode numbers m dominant in the power spectrum.

The power spectrum is mostly localized at the shear layer region, although important levels of fluctuations are also encountered at large values of r . As the fluctuation energy appears in low mode numbers, the cylindrical geometry becomes important. The vorticity gradient term $k_y v_y''(x)$ in the Rayleigh equation (Kelvin-Helmholtz instability) is replaced by $(m/r) \frac{d}{dr} \left[\frac{1}{r} \frac{d}{dr} (r^2 \Omega) \right]$ in the cylindrical plasma with angular rotation frequency $\Omega = v_\theta/r$. The stability analysis [12, 13] shows that the centrifugal force acts as an effective gravity $g_0 \mathbf{r}/a$ giving rise to the Rayleigh-Taylor instability partially controlled by the Coriolis force effect $2m\Omega$ and shear flow. In the simplest case of solid body rotation and a gaussian density model $n(r) = n_0 e^{-r^2/a^2}$ the stability is given by $A\tilde{\omega}^2 + B\tilde{\omega} + C = 0$ where $\tilde{\omega}$ is the Doppler shifted frequency $\omega - m\Omega$. The coefficients are $A = \nu_{m,n}(b/a) + A_p$ where b is the radius of the surrounding conducting wall and $A_p \propto k_{\parallel}^2$ measures the divergence of the parallel electron current, $B = 2m\Omega - A_p \omega_{*e}$ from the Coriolis effect and the density gradient $\omega_{*e} = -(mT_e/eBr) \frac{d}{dr} \ln n_0(r)$ and $C = m^2(\Omega^2 + g_0/a)$ the interchange instability (in a straight, axial B_z laboratory plasma $g_0 = 0$). The stability of the $m = 1$ and $m = 2$ modes depend on how close the conducting wall is to the plasma radius and the details are contained in the eigenvalue $\nu_{m,n} = m + 2n + f(b/a)$ where m, n are the azimuthal and radial eigenmode numbers and $f(b/a) \rightarrow 0$ as the conducting wall moves to infinity, $b/a \rightarrow \infty$.

Examples of the eigenfunctions and eigenvalues as function of the wall-to-plasma radius and the shear in the rotation frequency $\Omega(r)$ for the modes $m = 1, 2$ and 3 are shown in [12]. This stability analysis suggests that the large density fluctuation observed in the edge are associated with lower m modes driven by the centrifugal force acting on the density gradient.

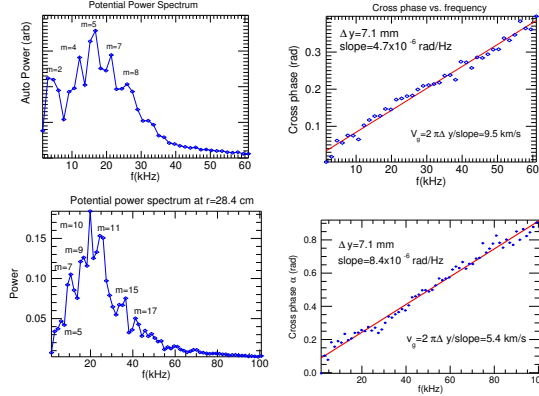


FIG. 6: Top left: Auto power spectrum for plasma potential at the center of the shear layer in the KH regime. Top right: Cross phase between two angularly separated probes for the KH regime. Bottom left: Auto power spectrum for plasma potential at the center of the shear layer in the DWKH regime. Bottom right: Cross phase between two angularly separated probes for the DWKH regime.

III. LINEAR DISPERSION RELATIONS

Previous section spectral analysis showed evidence of non-dispersive wave propagation in the frequency range between 5 kHz to 60 kHz in both regimes. Linear dispersion relation for simple theoretical profiles have been determined in [14] for the step-up flow profile in the DWKH regime and in [7] for a triangular piecewise linear jet in the KH regime. Dispersion relations are shown in Fig. 7.

An early study of the KH mode in small laboratory devices include Kent *et. al.* [15] with a Q-machine with $L/a = 100\text{cm}/1\text{cm} = 100$, $B = 0.1$ to 0.4 T at $T_e = 0.2$ eV, and $n = 5 \times 10^8$ to $5 \times 10^{10} \text{ cm}^{-3}$. Kent *et. al.* conclude that the edge oscillations over 5 kHz in frequency where $\Omega_{max} = 2 \times 10^4$ rad/s at the edge are KH modes and caution neglecting these modes in the stability of lower frequency drift waves.

In the larger Columbia Linear Machine (CLM) Sen *et. al.* [16] report the identification of KH modes at the frequency of 65 kHz. In the CLM with $L/a = 100 \text{ cm}/3 \text{ cm} = 50$, $B = 0.1$ to 0.15 T and $Te \sim Ti \sim 5$ eV, $n \sim 5 \times 10^8$ to $5 \times 10^9 \text{ cm}^{-3}$, the KH instability is a permanent feature in the region of maximum Er which has a laboratory frequency of 55 to 65 kHz.

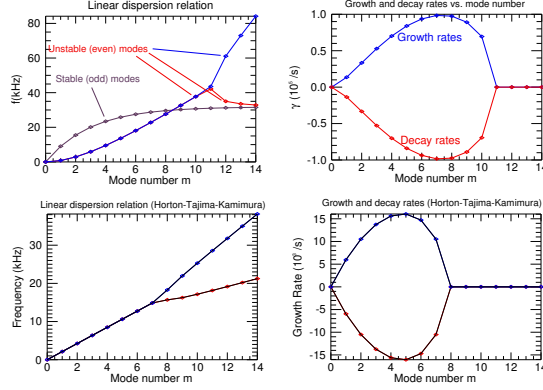


FIG. 7: Top left: Linear dispersion relation from Rayleigh equation for a triangular jet for KH instability. Top right: Growth and decay rates for the triangular jet. Bottom left: Top right: Linear dispersion relation from Rayleigh equation for a step-up sheared flow. Bottom right: Growth and decay rates for the step-up sheared flow profile

IV. CONCLUSIONS

Measurements of ρ_s -scale vorticity fluctuations were reported in the sheared rotation experiment in the LArge Plasma Device facility at UCLA. Vorticity measurements show evidence for the existence of coherent structures in two different sheared flow regimes at the edge of the plasma column. In the first regime, a localized plasma jet drives the Kelvin-Helmholtz instability giving rise to a chain of counter rotating vortices with signs being consistent with the antisymmetric background vorticity profile. Evidence of this is shown in the heavy tails present in the vorticity probability distribution functions and the sign change of the corresponding skewness across the shear layer. In the second regime, a step-up shear profile, with weaker rotation speed, drives drift wave instability in the presence of a sheared flow. Here, the vorticity probability distribution functions still show heavy tails but with no apparent skewness.

Spectral analysis of the turbulent data showed the existence of coherent waves propagating around the axis of the machine with speeds of the order of the rotation speed. Mode numbers are determined from cross phase plots which are in good agreement with the most unstable modes previously predicted by linear theory. However, once the modes saturate and the nonlinearity takes over, an inverse cascade process from the merging of like-sign vortices will transfer the energy to the lower mode numbers, explaining the dominance by low mode numbers in the fluctuation spectrum.

ACKNOWLEDGMENTS

The authors would like to thank J.E. Maggs, R.J. Taylor, and P. Pribyl for assistance with the biased rotation experiments on LAPD and M. Fassler for technical assistance in the construction of the vorticity probe.

The work was supported under the U.S. Department of Energy contract DE-FG02-04ER 54742. Experimental work was performed at the UCLA Basic Plasma Science Facility which is funded by NSF and DOE.

-
- [1] G. K. Batchelor. *An introduction to fluid mechanics*. Cambridge, 1967.
 - [2] L. D. Landau and E. M. Lifshitz. *Fluid Mechanics*. Pergamon, 1979.
 - [3] S. Chandrasekar. *Hydrodynamics and Hydromagnetic Stability*. Dover, 1961.
 - [4] A. Hasegawa and K. Mima. *Phys. Fluids*, 21(1), 1978.
 - [5] A. Hasegawa and M. Wakatani. *Phys. Rev. Lett.*, 50:682, 1983.
 - [6] S. Hamaguchi and W. Horton. *Phys. Fluids B*, 4(2), 1992.
 - [7] W. Horton, Jean C. Perez, T. Carter, and R. Bengston. *Physics of Plasmas*, 12(022303), 2005.
 - [8] W. Gekelman, H. Pfister, Z. Lucky, J. Bamber, D. Leneman, and J. Maggs. *Rev. Sci. Instrum.*, 62(12):2875–2883, 1991.
 - [9] M. Abramowitz and I. Stegun. *Handbook of Mathematical Functions*. Dover, 1970.
 - [10] E. J. Powers. *Nucl. Fus.*, 14:749, 1974.
 - [11] D. E. Smith and E. J. Powers. *Phys. of Fluids*, 16:1373, 1973.
 - [12] J. Liu, W. Horton, and J. E. Sedlak. *Phys. Fluids*, 30(2):467, 1987.
 - [13] W. Horton and J. Liu. *Phys. Fluids*, 27(8):2067, 1984.
 - [14] W. Horton, T. Tajima, and T. Kamimura. *Phys. Fluids B*, 30:3485–3495, 1987.
 - [15] G. Kent, N. Jen, and F. F. Chen. *Phys. Fluids*, 12(10):2140, 1969.
 - [16] A. K. Sen, V. Reva, and K. Avinash. *Physics of Plasmas*, 8(11):4772, 2001.